Available online at www.sciencedirect.com
ScienceDirect
Applied Catalysis B: Environmental 78 (2008) 120–128
APPLIED CATALYSIS B: ENVIRONMENTAL
www.elsevier.com/locate/apcatb

Preparation, characterization and catalytic behavior of nanostructured mesoporous $CuO/Ce_{0.8}Zr_{0.2}O_2$ catalysts for low-temperature CO oxidation

Jian-Liang Cao [a], Yan Wang [b], Tong-Ying Zhang [b], Shi-Hua Wu [b], Zhong-Yong Yuan [a,*]

[a] *Institute of New Catalytic Materials Science, College of Chemistry, Nankai University, Tianjin 300071, China*
[b] *Department of Chemistry, Nankai University, Tianjin 300071, China*

Received 6 June 2007; received in revised form 27 August 2007; accepted 12 September 2007
Available online 18 September 2007

Abstract

High-surface area mesoporous $CuO/Ce_{0.8}Zr_{0.2}O_2$ catalysts were prepared by a surfactant-assisted method of nanocrystalline particle assembly, and characterized by XRD, N_2 adsorption, TEM, H_2-TPR, TG-DTA and XPS techniques. The catalytic properties of the $CuO/Ce_{0.8}Zr_{0.2}O_2$ nanocatalysts were evaluated by low-temperature carbon monoxide oxidation using a microreactor-GC system. XRD and TEM analysis indicated that the catalyst particles were nanoscaled with cubic, fluorite structure. N_2 adsorption–desorption isotherms revealed a mesoporous nanocatalyst system with high-surface area and uniform pore-size distribution. The results of catalytic activity measurements showed that these mesoporous nanostructured $CuO/Ce_{0.8}Zr_{0.2}O_2$ catalysts were very active for low-temperature CO oxidation. The catalytic behavior depended on the CuO loading amount, the calcination temperature, the surface area and the particle size of the catalyst. The catalyst with 25 mol% CuO loading and calcined at 400 °C exhibited the highest catalytic activity.

Keywords: $CuO/Ce_{0.8}Zr_{0.2}O_2$ catalysts; Mesoporous; Nanostructured; Low-temperature CO oxidation; Catalytic activity

1. Introduction

As the major air pollutant, carbon monoxide is usually emitted from many industrial process, transportation and domestic activities. It is harmful to human health and environment. In order to control the toxic emission, catalytic oxidation of CO is an efficient way. During the last decades, a number of catalysts have been studied, in which precious metal catalysts such as Pd/SnO_2, Au/MnO_x, $Au/\alpha\text{-}Fe_2O_3$, Pt/SnO_2 and Au/SnO_2 have been demonstrated to be very effective [1–5]. Although the precious metal catalysts have high activity for CO oxidation, the high cost and limited availability discourage their extensive applications. Much attention has thus recently been paid to base metal as catalysts, especially copper oxide [6–10], for the purpose to find an alternative catalytic component to reduce using or even replace the noble metal.

Cerium dioxide is of great interest for its important applications including three-way catalysts for automotive exhaust gas treatment. Oxygen storage and release properties are the most important function of CeO_2, which provided by the redox couple "Ce^{4+}/Ce^{3+}" making more oxygen available for the oxidation process [11]. Cerium dioxide supported precious metal and CuO catalysts were used for carbon monoxide oxidation [10,12,13]. However, it is known that the pure CeO_2 has poor thermal stability. The structure modification of the CeO_2 lattice by doping with transition metal oxides may improve the stability of the ceria surface at high temperature [14]. Recently, Ce-containing mixed oxides, such as CeO_2-Al_2O_3, CeO_2-SiO_2, CeO_2-La_2O_3, CeO_2-SnO_2 and CeO_2-TiO_2 were reported for the use as oxidation catalysts [15–18]. It has been reported that the addition of ZrO_2 to CeO_2 can control the structure or the sites of CeO_2 crystallite and form a Ce-Zr-O solid solution, which leads to improvement in oxygen storage capacity (OSC) of CeO_2, redox property, thermal resistance and promotion of metal dispersion [19–24], resulting in better performance in CO oxidation [25] and combustion of methane [26]. Chen et al. [27] systematically investigated the effects of different Ce/Zr ratio for the $Ce_xZr_{1-x}O_2$ materials. Trovarelli et al. [28] suggested that the $Ce_{0.8}Zr_{0.2}O_2$ was the most texturally stable composition.

* Corresponding author. Tel.: +86 22 23509610; fax: +86 22 23509610.
E-mail address: zyyuan@nankai.edu.cn (Z.-Y. Yuan).

0926-3373/$ – see front matter © 2007 Elsevier B.V. All rights reserved.
doi:10.1016/j.apcatb.2007.09.007

CuO supported on CeO_2 and Ce-Zr-O enhances CO oxidation activity through a synergistic effect. Some methods, such as deposition–precipitation, co-precipitation, impregnation, and sol–gel methods [12,29–33], have been used for the preparation of such supported catalysts with different morphology and dispersion of copper species. However, little attention has been paid to the formation of mesoporous structure of Ce-Zr-O catalyst supports, though the mesoporous support would give rise to well-dispersed and stable metal catalyst particles on the surface upon calcination and reduction because of its abundant pores and large surface area, exhibiting a great potential in further improving the catalytic performance [34]. The catalysts having high-surface area and nanoscaled particle size could provide numerous, more reactive sites, so as to enhance the catalytic activity. In this paper, we report for the first time the preparation of mesoporous nanostructured CuO/$Ce_{0.8}Zr_{0.2}O_2$ catalysts by a surfactant-assisted method for CO oxidation at low temperature. The textural and structural properties of the prepared CuO/$Ce_{0.8}Zr_{0.2}O_2$ nanocatalysts were characterized by means of XRD, N_2 sorption, TEM, H_2-TPR, TG-DTA and XPS. The effect of the CuO content and calcination temperature on the catalytic activity of the mesoporous CuO/$Ce_{0.8}Zr_{0.2}O_2$ catalysts were investigated in detail.

2. Experimental

2.1. Catalyst preparation

The CuO/$Ce_{0.8}Zr_{0.2}O_2$ catalysts with different CuO content were synthesized using a surfactant-assisted method of nanoparticle assembly. At room temperature, 6 mmol of cetyltrimethylammonium bromide (CTAB) was dissolved into 200 ml distilled water under ultrasound irradiation for 15 min, then 8 mmol of $Ce(NO_3)_3{\cdot}6H_2O$, 2 mmol of $Zr(NO_3)_4{\cdot}5H_2O$ and calculated amount of $Cu(NO_3)_2{\cdot}3H_2O$ were added under vigorous stirring. After stirring for 0.5 h, 0.2 mol/l sodium hydroxide solution was gradually added into the above solution until the pH value of the mixed solution was 10, and then further stirred for about 12 h. The final suspended solution was aged at 90 °C for 3 h, washed with hot water, dried in the oven at 110 °C for 6 h, then milled and calcined at 400 °C for 4 h. The content of CuO was 0, 5, 10, 15, 20, 25, 30, 40 mol%, and the corresponding catalysts were denoted as CeZrCu0, CeZrCu5, CeZrCu10, CeZrCu15, CeZrCu20, CeZrCu25, CeZrCu30, CeZrCu40, respectively. In order to make clear the influence of the calcination temperature on the catalyst property, a series of CeZrCu25 catalysts calcined at different temperature were prepared in the similar manner.

2.2. Catalyst characterization

X-ray diffraction (XRD) analysis was performed on a Rigaku D/max-2500 diffractometer, with Cu Kα radiation at 40 kV and 100 mA in a scanning range of 3–80° (2θ). The diffraction peaks of the crystalline phase were compared with those of standard compounds reported in the JCPDS Date File. The average crystallite size was calculated from the peak width using the Scherrer's equation.

N_2 adsorption–desorption isotherms were collected at liquid nitrogen temperature using a Quantachrome NOVA 2000e sorption analyzer. The specific surface areas (S_{BET}) of the samples were calculated following the multi-point Brunauer–Emmett–Teller (BET) procedure. The pore-size distributions were determined from the adsorption branch of the isotherms using the Barett–Joyner–Halenda (BJH) method. Before carrying out the measurement, each sample was degassed at 200 °C for more than 6 h.

Transmission electron microscopy (TEM) analysis was performed on a Philips Tecnai G20 microscope, operating at 200 kV. The samples were dispersed in ethanol and treated with ultrasound for 5 min, and then deposited on a copper grid coated with preformed holey carbon film.

Temperature-programmed reduction (TPR) experiments were performed under the mixture of 5% H_2 in N_2 flowing (30 ml/min) over 50 mg of catalyst at a heating rate of 10 °C/min. The uptake amount during the reduction was measured by using a thermal conductivity detector (TCD). For comparison, H_2-TPR measurement of pure CuO was carried out over 7.4 mg of CuO powder.

Thermogravimetry-differential thermal analysis (TG-DTA) of the sample was conducted on a Rigaku Standard Model thermal analyzer in air atmosphere (flow rate: 90 ml/min; heat rate: 10 °C/min).

X-ray photoelectron spectroscopy (XPS) measurements were carried out on a Perkin-Elmer PHI 5600 spectrophotometer with the Mg Kα radiation. The operating conditions were kept constantly at 187.5 eV and 250.0 W. In order to subtract the surface charging effect, the C1s peak has been fixed at a binding energy of 284.6 eV.

2.3. Catalytic activity testing

Catalytic activity tests were performed in a continuous-flow fixed-bed microreactor. A stainless steel tube with an inner diameter of 7 mm was chosen as the reactor tube. About 200 mg catalyst power was placed into the tube. The reaction gas mixture consisting of 10 vol.% CO balanced with air was passed through the catalyst bed at a total flow rate of 36.6 ml/min. A typical weigh hourly space velocity (WHSV) was 11,000 ml/h/g. After 30 min reaction, the effluent gases were analyzed online by a GC-900A gas chromatograph equipped with a thermal conductivity detector. The activity was expressed by the conversion of CO.

3. Results and discussion

3.1. Catalyst characterization

3.1.1. X-ray diffraction and thermogravimetric analysis

X-ray diffraction patterns of the prepared CuO/$Ce_{0.8}Zr_{0.2}O_2$ catalysts with different CuO content are shown in Fig. 1. The main reflections at 28.8, 33.3, 47.9 and 56.8° of 2θ in the XRD patterns of all the samples correspond to the cubic, fluorite

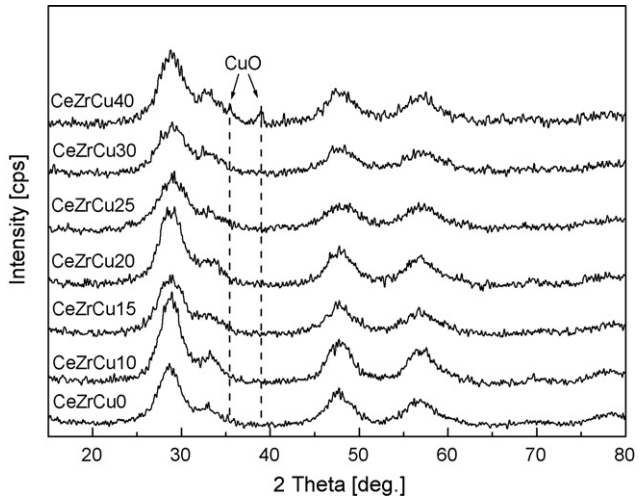

Fig. 1. XRD patterns of $CuO/Ce_{0.8}Zr_{0.2}O_2$ catalysts with different CuO contents calcined at 400 °C for 4 h.

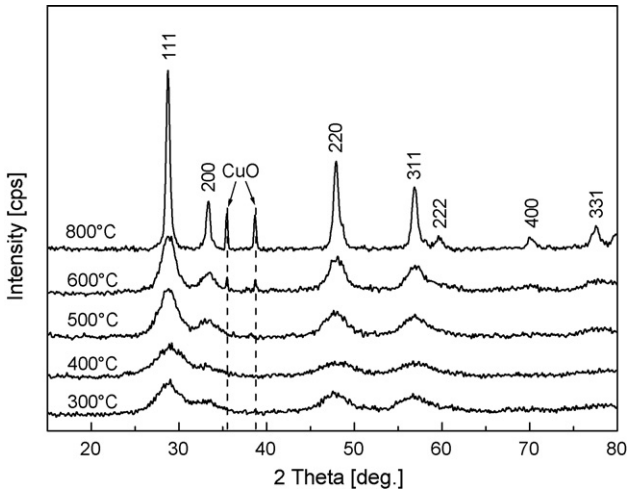

Fig. 3. XRD patterns of CeZrCu25 catalysts calcined at different temperatures.

structure typical of CeO_2, and there is no indication of the presence of other phases. This indicates that the zirconia dopant is contained within the lattice and formed a solid solution while maintaining the fluorite structure [29]. From Fig. 1, it can be seen that when the CuO content below 30 mol%, no reflections characteristic of CuO structure presented, which may be due to the high dispersion of the CuO nanoparticles with too small particle sizes on the surface of the support to be identified by the conventional X-ray diffraction method or the localization of Cu^{2+} ions in the solid solution of support. When the CuO content increased to 40 mol%, the weak diffraction peaks attributed to CuO crystal phase appeared at 35.5° and 38.7°. The average size of CuO particles in CeZrCu40 catalyst calcined at 400 °C, calculated from the CuO (1 1 1) reflection peak by the Scherrer formula, is 8.8 nm.

The TG-DTA result of the CeZrCu25 precursor is shown in Fig. 2. It can be seen that the endothermic peak between 75 and 175 °C on DTA, accompanied by a significant weight loss on TG, is attributed to the desorption of water (that may be physical or chemical adsorption on the interparticle surface of the sample or reside the mesopores). The main weight loss

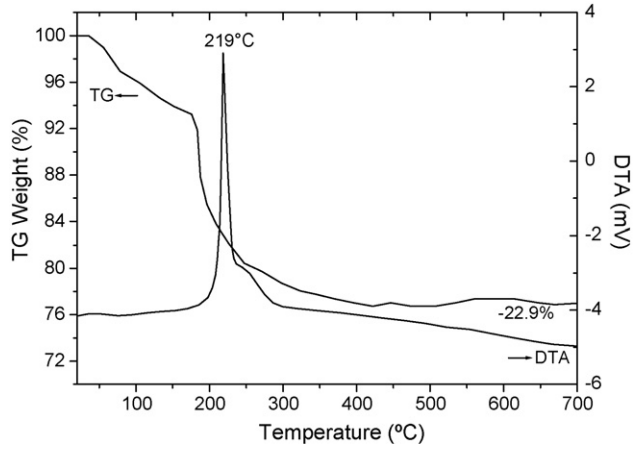

Fig. 2. TG/DTA patterns of the precursor of CeZrCu25 catalyst.

between 175 and 400 °C on the TG curve, accompanied with a strong exothermic peak at 219 °C and a shoulder around 255 °C, can be attributed to the decomposition of the surfactant and the combustion of carbon species. The total weight loss is 22.9 wt.%. No crystalline phase transformation is observed. After 400 °C, the weight of the precursor no longer changes, which indicates that the carbon species (surfactant molecules) in the samples could be completely removed after calcination at 400 °C in air. Since calcination at high temperature could result in decline in the surface area and increase in the crystallite size of catalysts, the feasible calcination temperature under air atmosphere was 400 °C for the $CuO/Ce_{0.8}Zr_{0.2}O_2$ catalysts.

The XRD patterns of CeZrCu25 catalysts calcined at different temperatures are presented in Fig. 3. With the increase of the precalcination temperature of the $CuO/Ce_{0.8}Zr_{0.2}O_2$ catalysts from 300 to 800 °C, a progressive increase in the relative intensity of the lines of $Ce_{0.8}Zr_{0.2}O_2$ phase is seen, indicating an increase of the degree of crystallinity and the particle size of $Ce_{0.8}Zr_{0.2}O_2$ support by the thermal treatment. Two weak diffractions characteristic of CuO structure at 35.5° and 38.7° (2θ) can be observed when the catalysts calcined at 600 °C or above, which became a little sharp when the calcination temperature was 800 °C, suggesting the growth of the CuO nanoparticles after high-temperature-calcination of the catalyst system. The mean particle sizes of $Ce_{0.8}Zr_{0.2}O_2$, calculated by the Scherrer's equation with the half width of the diffraction peak of the (1 1 1) plane are listed in Table 1. It is seen that the mean particle sizes of $Ce_{0.8}Zr_{0.2}O_2$ are in the range of 2.2–4.3 nm when the catalyst systems were calcined in the temperature range of 300–600 °C. Meanwhile, the mean particle size of CeZrCu25 calcined at 800 °C increased to 17.9 nm. The average sizes of CuO particles in CeZrCu25 catalysts calcined at 600 and 800 °C, calculated from the CuO (1 1 1) reflection peak, are 14.7 and 28.9 nm, respectively.

3.1.2. N_2 adsorption analysis and transmission electron microscopy

The nitrogen adsorption–desorption isotherms and the corresponding pore size distributions of the catalysts with

Table 1
Comparison of particle sizes, textural properties, and catalytic activities for CO oxidation of $CuO/Ce_{0.8}Zr_{0.2}O_2$ (CeZrCu*x*) catalysts

Catalysts	Calcination temperature (°C)	Mean particle size of $Ce_{0.8}Zr_{0.2}O_2$ (nm)	Mean particle size of CuO (nm)	Surface area[a] (m^2/g)	Pore volume[b] (cm^3/g)	$D_{BJH\text{-}ads}$[c] (nm)	$D_{BJH\text{-}des}$[d] (nm)	Average pore diameter[e] (nm)	CO conversion% (T/°C)
CeZrCu0	400	2.8	–	239	0.215	2.6	3.8	3.6	28.98 (260)
CeZrCu10	400	2.9	–	226	0.226	2.5	3.7	4.0	100 (130)
CeZrCu15	400	2.3	–	191	0.148	2.3	3.5	3.1	100 (105)
CeZrCu20	400	2.6	–	190	0.174	2.2	3.5	3.7	100 (100)
CeZrCu25	400	2.3	–	183	0.149	2.0	3.7	3.3	100 (90)
CeZrCu30	400	2.2	–	138	0.095	1.8	1.9	2.8	100 (130)
CeZrCu40	400	2.6	8.8	127	0.104	1.9	2.1	3.3	100 (130)
CeZrCu25	300	2.3	–	157	0.127	1.8	3.7	3.2	100 (100)
CeZrCu25	500	3.1	–	131	0.117	2.5	3.8	3.6	100 (95)
CeZrCu25	600	4.3	14.7	70	0.077	3.4	3.7	4.4	100 (125)
CeZrCu25	800	17.9	28.9	7	0.026	3.5	2.4	14.5	57.57 (220)

[a] Multi-point BET surface area.
[b] Total pore volume at $P/P_0 = 0.99$.
[c] Maximum of BJH pore diameter as determined from the adsorption branch.
[d] Maximum of BJH pore diameter as determined from the desorption branch.
[e] BJH average pore diameter ($4V/A$).

different CuO content and calcined at different temperature are shown in Figs. 4 and 5; their textual properties are also listed in Table 1. The isotherms of all the surfactant-assisted prepared catalysts are of classical type IV, characteristic of mesoporous materials. A hysteresis loop with a sloping adsorption branch and a relatively sharp steep desorption branch is observed at high relative pressure (P/P_0) range. Such a well-defined hysteresis loop of H2-type indicates that the effective radii of the mesoporous bodies are heterogeneously distributed and the effective radii of the narrow entrances are of equal size [35]. The H2-type of the hysteresis loop is typical for wormhole-like mesostructures and hierarchical scaffold-like mesoporous structures formed by surfactant-assisted nanoparticle assembly [35,36].

The adsorption isotherms of the prepared catalysts exhibit a large increase in the P/P_0 range of 0.2–0.4, which is characteristic of capillary condensation within mesopores. The pore-size distribution curves of the $CuO/Ce_{0.8}Zr_{0.2}O_2$ catalysts with different CuO content, determined by the BJH method from the adsorption branch of the isotherms, exhibit one single narrow peak centered at 1.8–2.6 nm (Fig. 4), indicating the good homogeneity of the pores. With the increase of the CuO content from 0 to 40 mol%, the surface area of the catalyst decreased from 239 to 127 m^2/g (Table 1), accompanied with the decrease of the pore volume and pore size. This may due to the agglomeration of CuO nanoparticles on the $Ce_{0.8}Zr_{0.2}O_2$ support. The pore size distributions of the CeZrCu25 catalysts calcined at different temperature are also narrow, and the pore sizes enlarged with the increase of

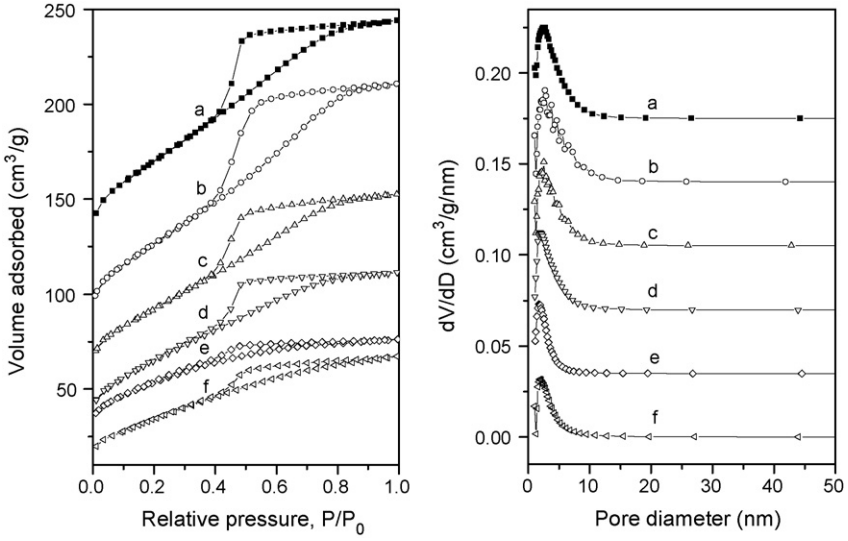

Fig. 4. (Left) N_2 adsorption–desorption isotherms and (right) the corresponding pore-size distribution curves of the $CuO/Ce_{0.8}Zr_{0.2}O_2$ catalysts with different CuO contents: (a) CeZrCu0, (b) CeZrCu10, (c) CeZrCu20, (d) CeZrCu25, (e) CeZrCu30, and (f) CeZrCu40. The volume was shifted by 105, 65, 40, 15 and 15 for the curves of data sets (a–e) and the dV/dD value was shifted by 0.175, 0.14, 0.105, 0.07 and 0.035 for the curves of data sets (a–e), respectively.

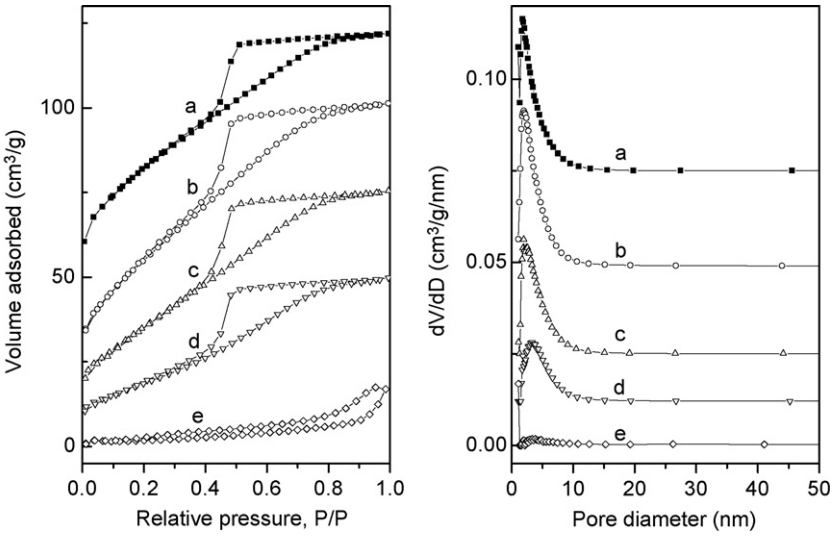

Fig. 5. (Left) N_2 sorption–desorption isotherms and (right) the corresponding pore-size distribution curves of the CeZrCu25 catalysts calcined at different temperature: (a) 300 °C, (b) 400 °C, (c) 500 °C, (d) 600 °C, and (e) 800 °C. The volume was shifted by 40 and 5 for the curves of data sets (a and b) and the d*V*/d*D* value was shifted by 0.075, 0.049, 0.025 and 0.012 for the curves of data sets (a–d), respectively.

calcination temperature (Fig. 5). The average pore diameters of the CeZrCu25 catalysts enlarged from 3.2 to 4.4 nm with the increase of calcination temperature from 300 to 600 °C, while the surface areas decreased from 183 to 70 m^2/g (Table 1). Interestingly, high surface area of 70 m^2/g can be obtained after calcination at 600 °C for 4 h, indicating the high thermal stability of these surfactant-assisted synthesized $CuO/Ce_{0.8}Zr_{0.2}O_2$ catalysts. The calcination at 800 °C resulted in the collapse of the mesoporous structure, and the surface area was only 7 m^2/g.

Fig. 6 shows the TEM micrographs of the sample CeZrCu0 and CeZrCu25 calcined at 400 °C. The images clearly demonstrate that the $CuO/Ce_{0.8}Zr_{0.2}O_2$ catalysts have a disordered wormhole-like mesopore structure, formed by the agglomeration of the uniform nanoparticles. The accessible pores are connected randomly, lacking discernible long-range order in the pore arrangement among the small $CuO/Ce_{0.8}Zr_{0.2}O_2$ particles, being in well agreement with the N_2 adsorption–desorption isotherms. The nanoparticles in these two samples are of regular shapes with the size around 3 nm, consistent with the crystallite size obtained by XRD.

3.1.3. H_2-TPR and X-ray photoelectron spectroscopy

In order to determine the existence state of copper species supported on $Ce_{0.8}Zr_{0.2}O_2$, the H_2-TPR analysis was performed. Fig. 7 shows the typical H_2-TPR profiles of $CuO/Ce_{0.8}Zr_{0.2}O_2$ catalyst (marked as CeZrCu25) and pure $Ce_{0.8}Zr_{0.2}O_2$ (marked as CeZrCu0) calcined at 400 °C, and the reduction profile of pure CuO powder is also presented for comparison. The pure $Ce_{0.8}Zr_{0.2}O_2$ has two reduction peaks at about 470 and 550 °C, ascribed to the reduction of surface and bulk oxygen of $Ce_{0.8}Zr_{0.2}O_2$, respectively. While the $CuO/Ce_{0.8}Zr_{0.2}O_2$ catalyst shows mainly two strong reduction peaks (α and β) at about 186 and 223 °C, besides a very weak peak around 580 °C. TPR curve of pure CuO shows a single peak of maximum hydrogen consumption at about 373 °C,

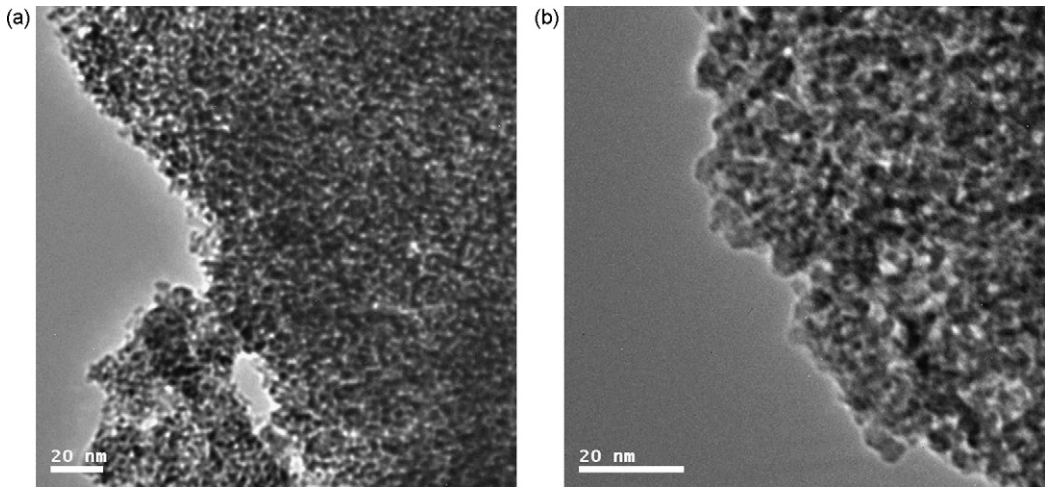

Fig. 6. TEM images of mesoporous (a) CeZrCu0 and (b) CeZrCu25 catalysts calcined at 400 °C for 4 h.

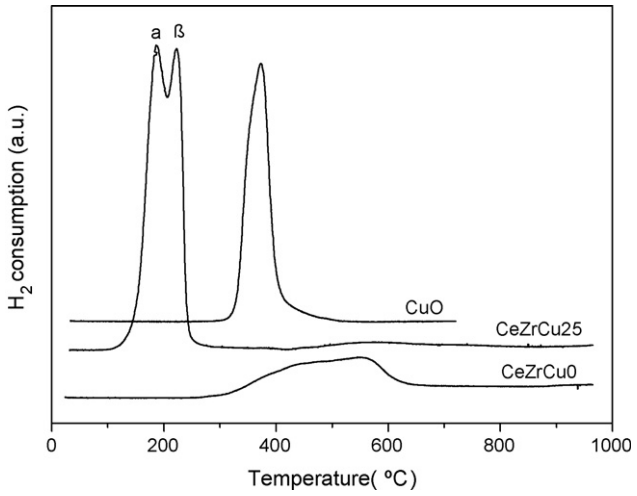

Fig. 7. H_2-TPR profiles of CuO, CeZrCu0 and CeZrCu25 catalysts calcined at 400 °C for 4 h.

which is in agreement with the previous report results [18,37]. Several groups have reported that there are two reduction peaks for copper species when CuO supported on the fluorite-type oxides [37–39], and these two reduction peaks are lower than the pure CuO. In the case of our study, the reduction peaks of copper species in the $CuO/Ce_{0.8}Zr_{0.2}O_2$ catalyst were also much lower than the pure CuO. This may be due to the synergistic effects between CuO and the $Ce_{0.8}Zr_{0.2}O_2$ support; $Ce_{0.8}Zr_{0.2}O_2$ is promoting the reduction of CuO. The lower temperature peak α for $CuO/Ce_{0.8}Zr_{0.2}O_2$ catalyst could be ascribed to the reduction of finely dispersed CuO species strongly interacting with the support [33,37], which are regarded as the active sites for CO oxidation. Considering no detection of CuO diffraction lines in the XRD pattern of CeZrCu25, and the possibility of the replacement of Ce^{4+} in $Ce_{0.8}Zr_{0.2}O_2$ solid solution by Cu^{2+} ions, the higher temperature peak β for $CuO/Ce_{0.8}Zr_{0.2}O_2$ catalyst could be assigned to the reduction of Cu^{2+} ions incorporated in the lattice of the $Ce_{0.8}Zr_{0.2}O_2$ support. The weak peak around 580 °C is assigned to the reduction of surface Ce^{4+} [18].

X-ray photoelectron spectroscopy was performed to illuminate the surface composition of the studied metal oxides and to acquire detailed information on the chemical states of the cations and anions. The spectra of Cu 2p, Ce 3d, Zr 3d and O 1s binding energies of the CeZrCu25 catalyst calcined at 400 °C are presented in Fig. 8. In Fig. 8a, the XPS peak centered at about 952.5 eV corresponds to Cu $2p_{1/2}$, and the peak at 932.5 eV with a shoulder at 933.8 eV corresponds to Cu $2p_{3/2}$. Avgouropoulos and Ioannides reported that the presence of shake-up peaks (about 939–944 eV) and a higher Cu $2p_{3/2}$ binding energy (about 933.0–933.8) are two major XPS characteristics of CuO, while a lower Cu $2p_{3/2}$ binding energy (about 932.2–933.1 eV) and the absence of the shake-up peak are the characteristics of reduced copper species [40]. In the case of the spectra of our catalyst, the presence of higher Cu $2p_{3/2}$ binding energy (about 933.8 eV) and the shake-up peak (about 938–942 eV) indicate the existence of Cu^{2+} species in the CeZrCu25 catalyst. Meanwhile, the lower Cu $2p_{3/2}$ binding energy (about 932.5 eV) is the characteristic of the reduced copper species. However, it is less convincing to distinguish between Cu_2O and Cu^0 because the Cu $2p_{3/2}$ binding energies and peak shapes of Cu_2O and Cu^0 are essentially identical. The formation of the reduced copper species may result from strong interaction of copper oxides with the high-surface area and nanosized Ce-Zr-O support [38] or the reduction of Cu^{2+} under the procedure of XPS measurement [7].

In Fig. 8b, Ce 3d spectrum shows six peaks at about 882.4, 889.3, 898.2, 900.7, 908.2 and 916.5 eV. The principal peaks of Ce $3d_{3/2}$ and Ce $3d_{5/2}$ are centered at about 900.7 and 882.4 eV, respectively. The peaks at 916.5 and 908.2 eV and the peaks at 898.2 and 889.3 eV are satellites arising from the Ce $3d_{3/2}$ and Ce $3d_{5/2}$, respectively. This is in agreement with the previous report of Ce^{4+} [41,42], indicating the main valence of Ce atom was +4. A small peak centered at about 885.6 eV indicates the presence of Ce^{3+}.

The peaks of Zr $3d_{5/2}$ and Zr $3d_{3/2}$ are centered at about 181.7 and 184.0 eV, respectively (Fig. 8c). The binding energy difference between the Zr $3d_{5/2}$ and Zr $3d_{3/2}$ photoemission feature is 2.3 eV. This value is in excellent agreement with the reported value [41]. The XPS spectrum for O 1s peak of CeZrCu25 catalyst (Fig. 8d) shows a main peak centered at 529.4 eV and a broad shoulder at about 531.2 eV, which indicates the existence of two different oxygen species. The position of the primary O 1s feature (ca. 529.4 eV) is assigned to the lattice oxygen associated with metal oxides, and the shoulder at about 531.2 eV is attributed to the chemisorbed oxygen [43].

The surface composition of the CeZrCu25 catalyst is estimated by XPS. The surface atomic contents of Cu, Ce and Zr are 6.68, 15.77 and 5.75%, respectively. The surface atomic ratio of Cu/(Cu + Ce + Zr) is 0.237, which is approximately consistent with the nominal atomic ratio (0.25).

3.2. Catalytic activity

The catalytic activities of the prepared $CuO/Ce_{0.8}Zr_{0.2}O_2$ catalysts as a function of reaction temperature are investigated and the results are presented in Figs. 9 and 10. The results show a similar behavior that the CO oxidation activity of all the $CuO/Ce_{0.8}Zr_{0.2}O_2$ samples increased with the increase of the catalytic reaction temperature measured in the catalyst bed. The "light-off" temperature for 100% CO conversion of the catalysts and the highest conversion of the catalysts which cannot reach 100% conversion in the present reaction condition are shown in Table 1.

Fig. 9 shows the catalytic activity of $CuO/Ce_{0.8}Zr_{0.2}O_2$ catalysts (CeZrCu*x*) with different content of CuO. The catalytic activity of pure $Ce_{0.8}Zr_{0.2}O_2$ support (CeZrCu0) is also included in the same figure for comparison purpose. It is noted from Fig. 9 that the activity of pure $Ce_{0.8}Zr_{0.2}O_2$ support is quite low (the pure CuO had no activity under the present condition), while the activities of all the $CuO/Ce_{0.8}Zr_{0.2}O_2$ catalysts are much higher than that of pure $Ce_{0.8}Zr_{0.2}O_2$. This illuminates that there is a synergistic effect between CuO and the $Ce_{0.8}Zr_{0.2}O_2$ support, which strongly affect the catalytic

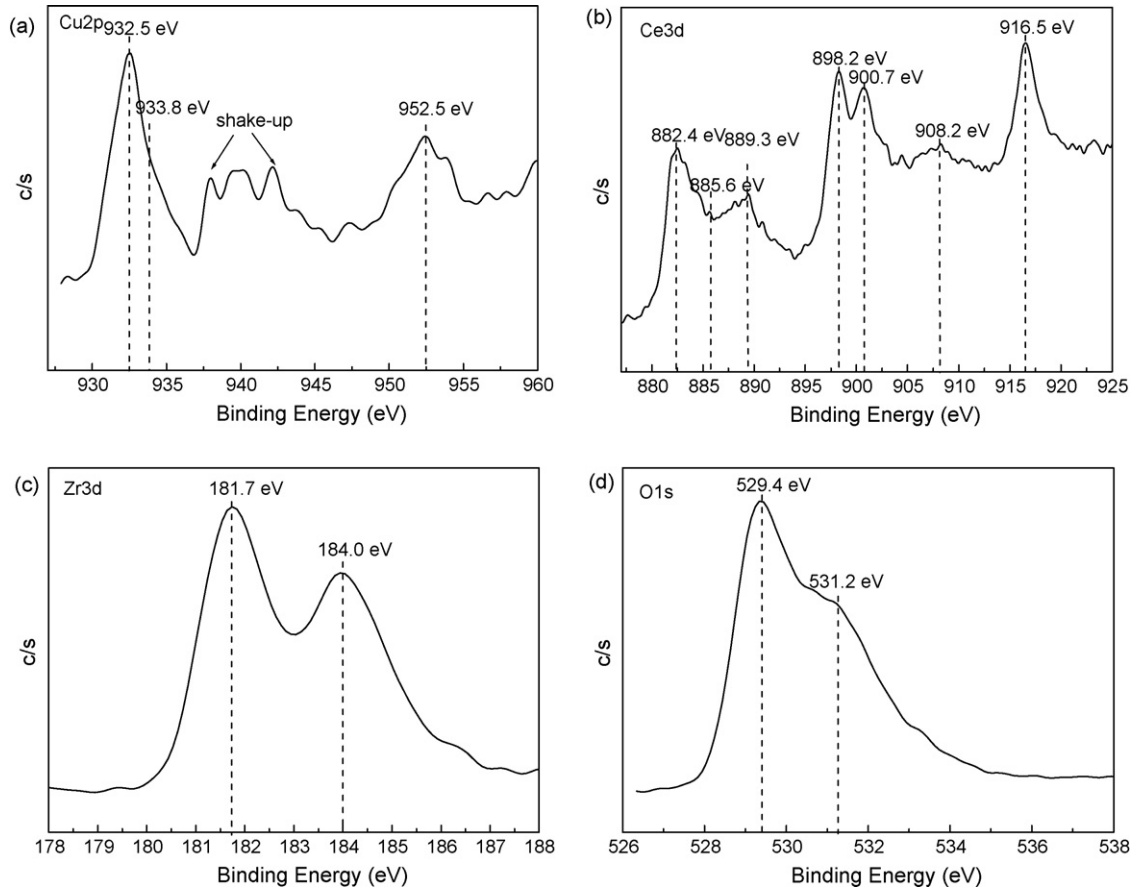

Fig. 8. XPS analysis of CeZrCu25 catalyst calcined at 400 °C: (a) Cu 2p spectrum, (b) Ce 3d spectrum, (c) Zr 3d spectrum, and (d) O 1s spectrum.

activity in low-temperature CO oxidation. The catalytic activity of $CuO/Ce_{0.8}Zr_{0.2}O_2$ catalysts enhanced with the increase of CuO loadings from 0 to 25 mol%, and the CeZrCu25 catalyst exhibited the highest catalytic activity. However, further increase of the CuO content resulted in the decrease of the catalytic activity. This indicates that the finely dispersed CuO species should be responsible for the activity, supported by the H_2-TPR and XRD results. The surface area and the pore volume of CeZrCu30 (138 m^2/g and 0.095 cm^3/g) were much lower than CeZrCu25 (183 m^2/g and 0.149 cm^3/g), though any significant difference cannot be observed between these two catalysts; while CeZrCu40 presented lower surface area than CeZrCu30 with the observable weak CuO diffraction peaks. This suggests that the CeZrCu25 has the largest monolayer

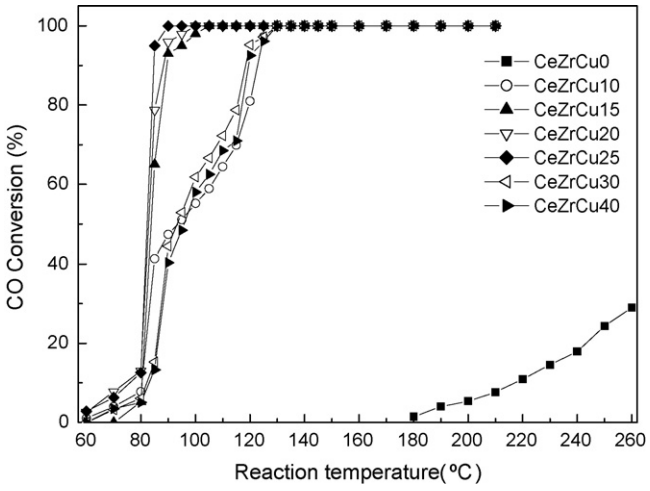

Fig. 9. Catalytic activity for CO oxidation of $CuO/Ce_{0.8}Zr_{0.2}O_2$ catalysts with different CuO contents calcined at 400 °C for 4 h.

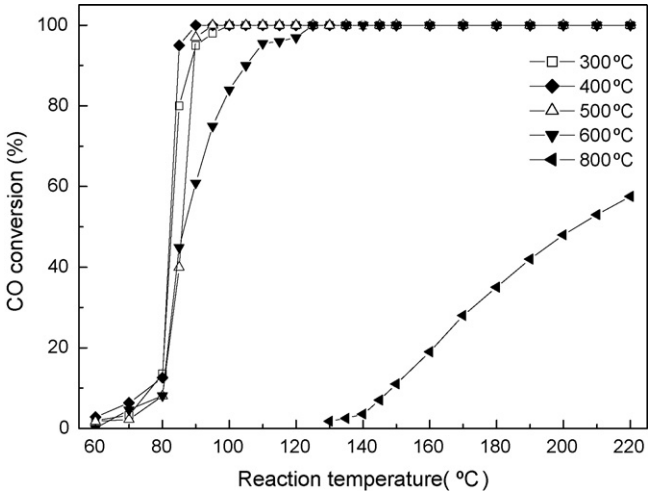

Fig. 10. Catalytic activity for CO oxidation of CeZrCu25 catalysts calcined at different temperatures for 4 h.

dispersion amount of CuO nanoparticles on the surface of $Ce_{0.8}Zr_{0.2}O_2$, presenting the largest active species with the lower reduction temperature, since the higher specific surface area of nanostructured catalysts could promote the higher dispersion of metal or oxide catalyst nanoparticles for the enhancing catalytic performance. When the high loading of CuO, the excess CuO species would not only cover some of the active sites, but also lead the grown CuO particles or bulk CuO formation, which maybe have negative effect on the catalytic activity of low-temperature CO oxidation. It is thus expected that the CuO particle size in CeZrCu30 might be a little larger than that in CeZrCu25, but still not enough large to be determinable by the XRD. At 40% of CuO loading, enlarged CuO particles were observed on the surface of $Ce_{0.8}Zr_{0.2}O_2$ support due to the excess CuO species, which may deteriorate the catalytic activity of the catalyst [31]. Therefore, the catalytic activity decreasing is observed from CeZrCu25 to CeZrCu30 to CeZrCu40.

Fig. 10 shows the catalytic performance for CO oxidation of CeZrCu25 catalysts calcined at different temperature. It is seen that the catalytic activity of the CeZrCu25 catalysts increased with the precalcination temperature from 300 to 400 °C, but decreased from 400 to 800 °C. This is supported by the TG-DTA data. Precalcination temperature of 300 °C can leave some carbon species of surfactant decomposition product that cover part of the active sites of the catalyst, resulting in the lower activity in 300 °C-calcined catalyst than the 400 °C-calcined one. When the reaction temperature is below 80 °C, the catalytic activities of the catalysts calcined at 300–600 °C are close to each other. Further increase the reaction temperature, the catalyst calcined at 600 °C shows lower activity than that calcined at 300, 400 and 500 °C. The CeZrCu25 catalyst calcined at 400 °C, which have the high surface area of 183 m^2/g and the particle size of 2.3 nm, exhibits the highest catalytic activity on CO oxidation with CO total conversion at 90 °C, which is higher than that of previously reported $CuO/Ce_{0.8}Zr_{0.2}O_2$ catalysts without mesopore structure [27,29,31]. The lower catalytic activity with the precalcination temperature increasing is related to the growth of the catalyst particles with the increase of precalcination temperature, accompanying with the surface area lowering. The XRD and nitrogen adsorption analysis has revealed that the heat treatment made the decrease of the surface areas and the increase of the $Ce_{0.8}Zr_{0.2}O_2$ and CuO particle sizes with the increase of calcination temperatures. The 600 °C-precalcination resulted in the CuO particle size enlarged to 14.7 nm with the catalyst surface area of only 70 m^2/g. The 800 °C-calcined CeZrCu25 catalyst has the lowest surface area of 7 m^2/g and the largest particle sizes (17.9 nm for $Ce_{0.8}Zr_{0.2}O_2$ and 28.9 nm for CuO) with the collapse of the mesoporous structure. The maximal CO conversion data on the CeZrCu25 catalyst calcined at 800 °C is 57.57% at the reaction temperature of 220 °C, which is the lowest one in all the catalysts we studied. Thus, the observed difference in the catalytic activities of the CeZrCu25 catalysts calcined at different temperature maybe due to the agglomeration of the catalysts, the decrease of the surface area, and the increase of the $Ce_{0.8}Zr_{0.2}O_2$ and/or CuO particle sizes by the increase of the calcination temperature. It is believed that high activity of these CeZrCux catalysts is corresponding to their high mesoporosity. The mesoporous frameworks provide a large surface to volume ratio, and hence more active sites are available for CO oxidation, benefiting to the enhanced catalytic activity, in comparison with those previous reported nonporous and low-surface-area $CuO/Ce_{0.8}Zr_{0.2}O_2$ catalysts [27,29,31].

4. Conclusions

Mesoporous nanostructured $CuO/Ce_{0.8}Zr_{0.2}O_2$ catalysts with high-surface areas and narrow mesopore size distributions have been prepared by the surfactant-assisted method of nanoparticle assembly. Only cubic, fluorite structure was observed for $Ce_{0.8}Zr_{0.2}O_2$. The catalysts containing CuO of larger than 30 mol% or calcined at temperature higher than 500 °C exhibited the CuO phase, which may have negative effect on the catalytic activity of low-temperature CO oxidation. The surface areas of the catalysts decreased sharply with the increasing of precalcination temperature. The XPS analysis indicated that reduced copper species presented in the catalysts and highly dispersed on the catalysts surface. The main valence of Ce atom was +4. The CO oxidation activity studies indicated that the content of CuO and precalcination temperature can affect the catalytic properties of the catalysts. The CeZrCu25 catalyst calcined at 400 °C has the highest catalytic activity. The synergistic effect between CuO and the $Ce_{0.8}Zr_{0.2}O_2$ support, the highly dispersed CuO nanoparticles, the mesoporous framework, the high-surface area and the uniform distribution of nanoscale particles size were responsible for the high catalytic activity of the catalysts for low-temperature CO oxidation.

Acknowledgements

This work was supported by the National Natural Science Foundation of China (Nos. 20473041 and 20673060), the National Basic Research Program of China (No. 2003CB615801), the Chinese-Bulgarian Scientific and Technological Cooperation Project, the Program for New Century Excellent Talents in University (NCET-06-0215), and Nankai University.

References

[1] D.R. Schryer, B.T. Upchurch, B.D. Sidney, K.G. Brown, G.B. Hoflund, R.K. Herz, J. Catal. 130 (1991) 314.
[2] M. Haruta, S. Tsubota, T. Kobayashi, H. Kageyama, M.J. Genet, B. Delmon, J. Catal. 144 (1993) 175.
[3] D.R. Schryer, B.T. Upchurch, J.D. Van Norman, K.G. Brown, J. Schryer, J. Catal. 122 (1990) 193.
[4] T. Engel, G. Ertl, Adv. Catal. 28 (1979) 1.
[5] S.R. Wang, J. Huang, Y.Q. Zhao, S.P. Wang, X.Y. Wang, T.Y. Zhang, S.H. Wu, S.M. Zhang, W.P. Huang, J. Mol. Catal. A 259 (2006) 245.
[6] B. Wen, M.Y. He, Appl. Catal. B 37 (2002) 75.
[7] H.Y. Zhu, M.M. Shen, Y. Kong, J.M. Hong, Y.H. Hu, T.D. Liu, L. Dong, Y. Chen, C. Jian, Z. Liu, J. Mol. Catal. A 219 (2004) 155.

[8] G. Avgouropoulos, T. Ioannides, H.K. Matralis, J. Batista, S. Hocevar, Catal. Lett. 73 (2001) 33.
[9] L. Dong, Y. Hu, M. Shen, T. Jin, J. Wang, W. Ding, Y. Chen, Chem. Mater. 13 (2001) 4227.
[10] X.-C. Zheng, S.-H. Wu, S.-P. Wang, S.-R. Wang, S.-M. Zhang, W.-P. Huang, Appl. Catal. A 283 (2005) 217.
[11] K. Min, M.W. Song, C.H. Lee, Appl. Catal. A 251 (2003) 143.
[12] C.R. Jung, J. Han, S.W. Nam, T.-H. Lim, S.-A. Hong, H.-I. Lee, Catal. Today 93–95 (2004) 183.
[13] X.-Y. Wang, S.-P. Wang, S.-R. Wang, Y.-Q. Zhao, J. Huang, S.-M. Zhang, W.-P. Huang, S.-H. Wu, Catal. Lett. 112 (2006) 115.
[14] A. Trovarelli, C. De Leitenburg, M. Boaro, G. Dolcetti, Catal. Today 50 (1999) 353.
[15] M.A. Centeno, C. Portales, I. Carrizosa, J.A. Odriozola, Catal. Lett. 102 (2005) 289.
[16] B.M. Reddy, A. Khan, P. Lakshmanan, M. Aouine, S. Loridant, J.C. Volta, J. Phys. Chem. B 109 (2005) 3355.
[17] H. Hu, J. Li, G.-H. Cheng, S. Li, J. Rare Earth 22 (2004) 470.
[18] R. Lin, M.-F. Luo, Y.-J. Zhong, Z.-L. Yuan, G.-Y. Liu, W.-P. Liu, Appl. Catal. A 255 (2003) 331.
[19] J.A. Wang, L.F. Chen, M.A. Valenzuela, A. Montoya, J. Salmoned, P.D. Angel, Appl. Surf. Sci. 230 (2004) 34.
[20] X.Y. Liu, S.D. Wang, Z.S. Yuan, J. Zhou, N. Liu, C.X. Zhang, G.Z. Fu, Chin. J. Catal. 25 (2004) 91.
[21] R. Si, Y.-W. Zhang, C.-X. Xiao, S.-J. Li, B.-X. Lin, Y. Kou, C.-H. Yan, Phys. Chem. Chem. Phys. 6 (2004) 1056.
[22] M. Daturi, E. Finocchio, C. Biinet, J.C. Lavalley, F. Fally, V. Perrichon, H. Vidal, N. Hickey, J. Kaspar, J. Phys. Chem. B 104 (2000) 9186.
[23] T. Masui, T. Ozaki, K. Machida, G. Adachi, J. Alloys Compd. 303 (2000) 49.
[24] E.S. Putna, T. Bunluesin, X.L. Fan, R.J. Gorte, J.M. Vohs, R.E. Lakis, T. Egami, Catal. Today 50 (1999) 343.
[25] M. Thammachart, V. Meeyoo, T. Risksomboon, S. Osuwan, Catal. Today 68 (2001) 53.
[26] C. Bozo, N. Guilhaume, E. Garbowski, M. Primet, Catal. Today 59 (2000) 33.
[27] Y.-Z. Chen, B.-J. Liaw, H.-C. Chen, Int. J. Hydrogen Energy 31 (2006) 427.
[28] A. Trovarelli, C. De Leitenburg, G. Dolcetti, ChemTech 27 (1997) 32.
[29] S.-P. Wang, X.-C. Zheng, X.-Y. Wang, S.-R. Wang, S.-M. Zhang, L.-H. Yu, W.-P. Huang, S.-H. Wu, Catal. Lett. 105 (2005) 163.
[30] P. Bera, S.T. Aruna, K.C. Patil, M.S. Hegde, J. Catal. 186 (1999) 36.
[31] S.-P. Wang, X.-Y. Wang, J. Huang, S.-M. Zhang, S.-R. Wang, S.-H. Wu, Catal. Commun. 8 (2007) 231.
[32] M. Jobbagy, M. Fernando, B. Schonbrod, G. Baronetti, M. Laborde, Chem. Mater. 18 (2006) 1945.
[33] M.-F. Luo, J.-M. Ma, J.-Q. Lu, Y.-P. Song, Y.-J. Wang, J. Catal. 246 (2007) 52.
[34] V. Idakiev, T. Tabakova, Z.Y. Yuan, B.L. Su, Appl. Catal. A 270 (2004) 135.
[35] Z.-Y. Yuan, B.-L. Su, Chem. Phys. Lett. 381 (2003) 710.
[36] T.-Z. Ren, Z.-Y. Yuan, B.-L. Su, Chem. Phys. Lett. 374 (2003) 170.
[37] M.-F. Luo, Y.-J. Zhong, X.-X. Yuan, X.-M. Zheng, Appl. Catal. A 162 (1997) 121.
[38] L. Kundakovic, M. Flytzani-Stephanopoulos, Appl. Catal. A 171 (1998) 13.
[39] P. Ratnasamy, D. Srinivas, C.V.V. Satyanarayana, P. Manikandan, R.S.S. Kumaran, M. Sachin, V.N. Shetti, J. Catal. 221 (2004) 455.
[40] G. Avgouropoulos, T. Ioannides, Appl. Catal. A 244 (2003) 155.
[41] A.E. Nelson, K.H. Schulz, Appl. Surf. Sci. 210 (2003) 206.
[42] Y.-W. Zhang, R. Si, C.-S. Liao, C.-H. Yan, C.-X. Xiao, Y. Kou, J. Phys. Chem. B 107 (2003) 10159.
[43] A. Platau, L.I. Johansson, A.L. Hagstrom, S.-E. Karlsson, S.B.M. Hagstrom, Surf. Sci. 63 (1997) 153.